Eur. Phys. J. C 26, 111–124 (2002)
Digital Object Identifier (DOI) 10.1140/epjc/s2002-01043-0

THE EUROPEAN PHYSICAL JOURNAL C

Neutrino indirect detection of neutralino dark matter in the CMSSM

V. Bertin[1,a], E. Nezri[1,2,b], J. Orloff[2,c]

[1] Centre de Physique des Particules de Marseille, IN2P3-CNRS, Université de la Méditerranée, 13288 Marseille Cedex 09, France
[2] Laboratoire de Physique Corpusculaire de Clermont-Ferrand, IN2P3-CNRS, Université Blaise Pascal, 63177 Aubiere Cedex, France

Received: 12 April 2002 / Revised version: 16 July 2002 /
Published online: 18 October 2002 –

Abstract. We study potential signals of neutralino dark matter indirect detection by neutrino telescopes in a wide range of CMSSM parameters. We also compare with direct detection potential signals taking into account in both cases present and future experiment sensitivities. Only models with neutralino annihilation into gauge bosons can satisfy cosmological constraints and current neutrino indirect detection sensitivities. For both direct and indirect detection, only next generation experiments will be able to really test this kind of models.

1 Introduction

Our present understanding of the universe is described in the framework of general relativity and cosmology. The densities of its components are related by [1]

$$\Omega(a) - 1 = \frac{\Omega_{\rm tot} - 1}{1 - \Omega_{\rm tot} + \Omega_\Lambda a^2 + \Omega_{\rm mat} a^{-1} + \Omega_{\rm rel} a^{-2}}, \quad (1)$$

where a is the scale factor. This equation and current experimental results suggest and focus on a flat universe with the parameters as given in Table 1 [2].

In the framework of the minimal supersymmetric standard model (MSSM) [3–7], the lightest supersymmetric particle (LSP) is typically the lightest of the neutralinos $\chi_1(\equiv \chi), \chi_2, \chi_3, \chi_4$, the mass eigenstates of the neutral gauge and Higgs boson superpartners $(\tilde{B}, \tilde{W}^3, \tilde{H}_d^0, \tilde{H}_u^0)$. In the rest of this paper, the LSP is thus assumed to be the lightest neutralino χ_1 and is called more generically χ. Assuming R-parity conservation ($R \equiv (-1)^{B+L+2S}$), the neutralino is a good stable candidate for cold dark matter [8]. In this context, all sparticles produced after the big bang give a neutralino in their decay chain, leading to a relic bath of χ in the present universe. These neutralinos could be observed via direct detection (χ interaction with a nucleus of a detector), or indirect detection of their annihilation products (ν, γ, $\bar{p}$, $\bar{D}$, e^+). We will mainly focus in this paper on indirect detection of ν. The relic neutralinos are gravitationally captured by massive astrophysical bodies and accumulated at the center of these objects by successive elastic scatterings on their nuclei. The captured neutralino population annihilates and gives rise to neutrino fluxes which could be detectable in neutrino telescopes like Amanda/Icecube, Antares, Baikal.

[a] e-mail: bertin@cppm.in2p3.fr
[b] e-mail: nezri@in2p3.fr
[c] e-mail: orloff@in2p3.fr

2 Neutralino in the CMSSM

In the MSSM, the mass matrix of neutralinos in the basis $(-\mathrm{i}\tilde{B}, -\mathrm{i}\tilde{W}^3, \tilde{H}_d^0, \tilde{H}_u^0)$ is (see (2) on top of the next page) where M_1, M_2 are mass terms of the $U(1)$ and $SU(2)$ gaugino fields, μ is the higgsino "mass" parameter and $\tan\beta = \langle H_u\rangle/\langle H_d\rangle$ is the ratio of the neutral Higgs vacuum expection values. The neutralino composition is

$$\chi = N_1\tilde{b} + N_2\tilde{W}^3 + N_3\tilde{H}_d^0 + N_4\tilde{H}_u^0, \quad (3)$$

and we define its gaugino fraction by $g_{\rm frac} = |N_1|^2 + |N_2|^2$.

In this model, the introduction of soft terms in the Lagrangian explicitly breaks supersymmetry, leading to a low energy effective theory with 106 parameters. The MSSM is therefore not very predictive, and a non-biased exploration of its parameter space is not possible. As a first step, we will therefore as usual concentrate on gravity-mediated supersymmetry breaking in supergravity [9] inspired models, with grand unification of soft terms at $E_{\rm GUT} \sim 2.10^{16}$ GeV parameterized by m_0 (common scalar mass), $m_{1/2}$ (common gaugino mass) and A_0 (common trilinear term). Together with $\tan\beta$ and $\mathrm{sgn}(\mu)$, these define a five-parameter constraint MSSM (CMSSM) or mSugra model [10–12], from which the 106 parameters can be deduced through renormalization group equations (RGEs).

Due to the large top Yukawa coupling, renormalization group evolution can drive $m_{H_u}^2|_{Q_{\rm EWSB}}$ and/or $m_{H_d}^2|_{Q_{\rm EWSB}}$

Table 1. Parameters for a flat universe

Cosmological constant:	$\Omega_\Lambda = 0.7 \pm 0.1$
Matter:	$\Omega_{\rm mat} = 0.3 \pm 0.1$
baryonic matter:	$\Omega_b = 0.04 \pm 0.01$; including $\Omega_{vis} \lesssim 0.01$
cold dark matter:	$\Omega_{DM} = 0.26 \pm 0.1$
Relativistic components:	$0.01 \lesssim \Omega_{\rm rel} \lesssim 0.05$
neutrinos:	$0.01 \lesssim \Omega_\nu \lesssim 0.05$
photons:	$\Omega_\gamma = 4.8^{+1.3}_{-0.9} \times 10^{-5}$
Hubble's constant:	$h \equiv H_0/100\ {\rm km^{-1}\ s^{-1}\ Mpc^{-1}} = 0.72 \pm 0.08$

$$M_{\chi,\chi_2,\chi_3,\chi_4} = \begin{pmatrix} M_1 & 0 & -m_Z\cos\beta\sin\theta_{\rm W} & m_Z\sin\beta\sin\theta_{\rm W} \\ 0 & M_2 & m_Z\cos\beta\cos\theta_{\rm W} & -m_Z\sin\beta\cos\theta_{\rm W} \\ -m_Z\cos\beta\sin\theta_{\rm W} & m_Z\cos\beta\cos\theta_{\rm W} & 0 & -\mu \\ m_Z\sin\beta\sin\theta_{\rm W} & -m_Z\sin\beta\cos\theta_{\rm W} & -\mu & 0 \end{pmatrix}, \quad (2)$$

to negative values, so that the electroweak symmetry breaking (EWSB) originates purely in quantum corrections, which realizes radiative electroweak symmetry breaking. Minimization of the scalar potential at the electroweak breaking scale $Q_{\rm EWSB}$ yields the condition

$$\begin{aligned} \frac{1}{2}m_Z^2 &= \frac{m_{H_d}^2|_{Q_{\rm EWSB}} - m_{H_u}^2|_{Q_{\rm EWSB}}\tan^2\beta}{\tan^2\beta - 1} \\ &\quad -\mu^2|_{Q_{\rm EWSB}} \\ &\sim_{\tan\beta\gtrsim 5} -m_{H_u}^2|_{Q_{\rm EWSB}} - \mu^2|_{Q_{\rm EWSB}}, \end{aligned} \quad (4)$$

where usually $Q_{\rm EWSB}$ is taken as $(m_{\tilde{t}_1}m_{\tilde{t}_2})^{1/2}$ [13] to minimize one-loop corrections.

Such mSugra models offer the theoretical advantage over generic MSSM models that problems such as Landau poles, charge and color breaking (CCB) minima are partially addressed when dealing with RGEs.

In mSugra, the lightest neutralino can exhibit two different natures, depending on the input parameter values [14,15]:

(1) an almost pure bino-like neutralino for low m_0, as the RGEs drive $M_1|_{Q_{\rm EWSB}} \simeq 0.41 M_1|_{\rm GUT} = 0.41 m_{1/2} \ll |\mu|_{Q_{\rm EWSB}}$ and $M_2|_{Q_{\rm EWSB}} \simeq 0.83 M_1|_{\rm GUT} = 0.83 m_{1/2} \ll |\mu|_{Q_{\rm EWSB}}$;

(2) for $m_0 \gtrsim 1000\,{\rm GeV}$, the neutralino picks up some higgsino mixing for $\tan\beta \gtrsim 5$ as the increase of m_0 drives $m_{H_u}^2$ to less negative values so that both $|m_{H_u}^2|$ and $|\mu|$ (via (4)) decrease. One can then have $|\mu|_{Q_{\rm EWSB}} \lesssim M_1|_{Q_{\rm EWSB}}$ depending on $m_{1/2}$. When $|\mu|$ is too small, EWSB cannot be achieved.

In addition, the very low m_0 values can lead to models with tachyonic sfermions (low $m_{1/2}$) or a slepton LSP. These behaviors are shown on Fig. 1 in the $(m_0, m_{1/2})$ plane. The neutralino mass is $\sim 0.4 m_{1/2}$ but is affected by low μ values at high m_0. Unless explicitly quoted we use $m_t = 174.3\,{\rm GeV}$.

In this paper, the RGE, SUSY spectrum and potential minimization are derived using the SUSPECT program [16,17] version 2.005 which includes two-loop RGEs [18], the tadpole method to minimize the scalar potential [19] and all radiative corrections in the mass spectrum [20]. The neutralino relic density, including $\chi\chi^+$ and $\chi\chi_2$ coannihilations and detection signals are calculated by the DarkSUSY (DS) package [21,22][1] which correctly implements s-channel poles and thresholds [23]. Our interface[2] shortcuts the DS spectrum recalculation, to comply with the SUSPECT spectra which have been checked [24] against SOFTSUSY [25].

3 Branching ratios in neutralino annihilation

The leading processes in neutralino annihilation at rest are shown in Fig. 2, where the last two processes are proportional to the higgsino/wino fraction of χ and $\chi_i^{(+)}$. In mSugra models, one can typically distinguish different regions of annihilation branching ratios in the $(m_0, m_{1/2})$ plane, for almost any values of $\tan\beta(\geq 5)$ (see Fig. 3).

3.1 Above top thresholds

We have above top thresholds i.e. $m_\chi \gtrsim m_{\rm top} \Leftrightarrow m_{1/2} \gtrsim 400\,{\rm GeV}$ or slightly higher in the mixed higgsino region.

3.1.1 Region I

For low m_0 (< 500–$1000\,{\rm GeV}$), the neutralino is almost purely bino-like. Despite a tiny higgsino fraction, its annihilation via the Z exchange amplitude, being proportional to the fermion mass, is surprisingly important in the top channel $\chi\chi \xrightarrow{Z} t\bar{t} \propto (m_t m_\chi/m_Z^2)^2 N_{3(4)}^2$. Another potentially important annihilation process is $\chi\chi \xrightarrow{A} b\bar{b}$, whose

[1] These calculations use a neutralino local density $\rho_\chi = 0.3\,{\rm GeV/cm^3}$ and a Maxwellian velocity distribution with $v_0 = 220\,{\rm km\,s^{-1}}$

[2] Available from nezri@in2p3.fr; submitted for inclusion in DS

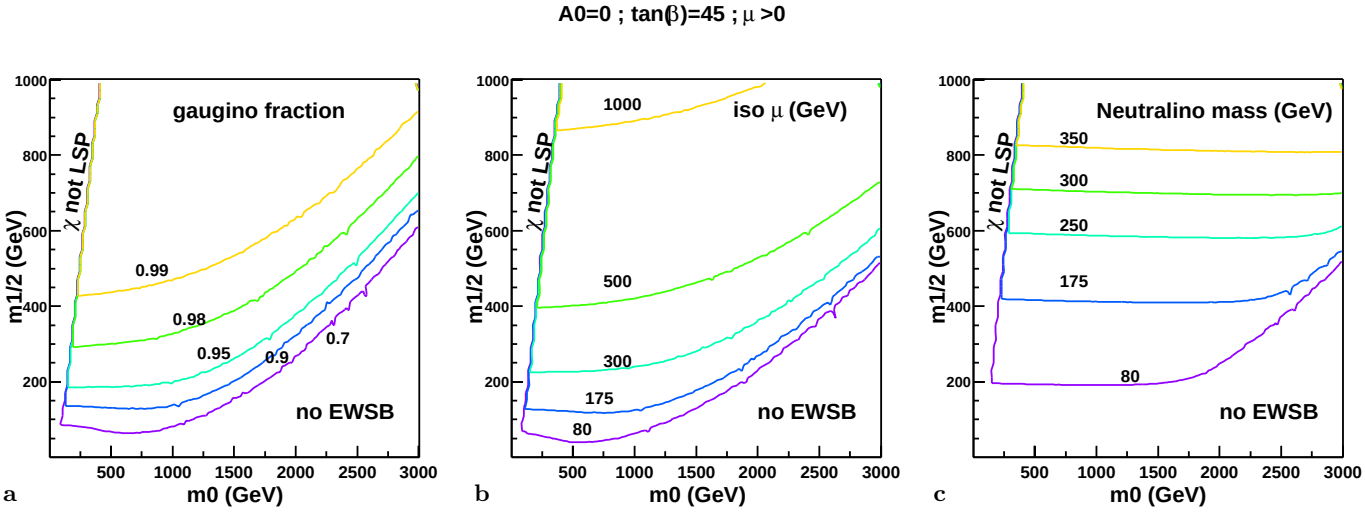

Fig. 1. **a** Gaugino fraction, **b** value of μ and **c** neutralino mass in the $(m_0, m_{1/2})$ plane. Region where χ is not the LSP or EWSB is not achieved are also indicated

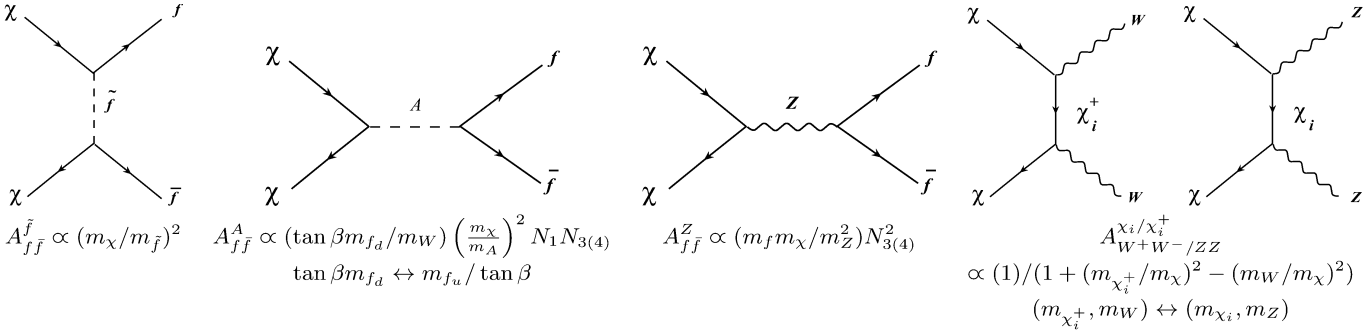

Fig. 2. Leading channels in neutralino annihilation at rest, with the parametric dependance of their amplitude, N_i being defined in (3) [8]

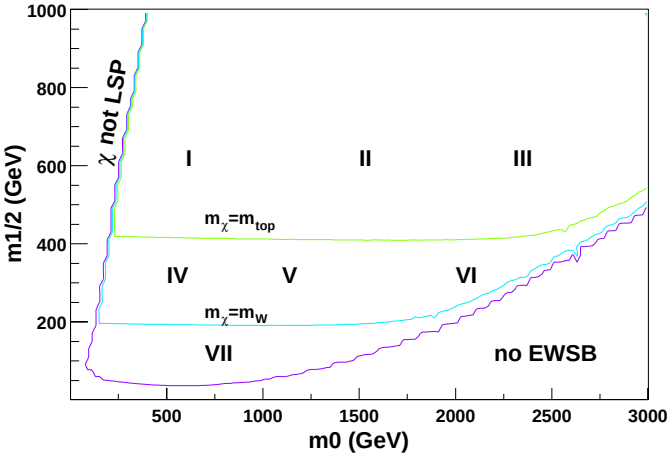

Fig. 3. Typical regions of neutralino annihilation

amplitude $|A^A_{b\bar{b}}| \propto (\tan\beta m_b/m_W)(m_\chi/m_A)^2 N_1 N_{3(4)}$ is strongly enhanced for high $\tan\beta$, both from the explicit dependence, and because m_A decreases when $\tan\beta$ increases. In the region of interest, their ratio $|A^Z_{t\bar{t}}/A^A_{b\bar{b}}|$ accordingly drops from $\sim$ 20–50 for $\tan\beta = 10$ down to $\sim$ 2–5 for $\tan\beta = 45$. Even taking the smaller $t\bar{t}$ phase space (a factor of 0.7) and the other subleading $b\bar{b}$ processes into account, the $b\bar{b}$ domination thus calls for an explanation on Fig. 4 and even more on Fig. 13. The only way to account for this domination is to recall the opposite sign of the $\chi\chi \xrightarrow{Z} t\bar{t}$ and $\chi\chi \xrightarrow{\tilde{t}} t\bar{t}$ amplitudes, thus allowing for a cancellation provided their order of magnitude match, which we checked analytically. The opposite happens for the annihilation into $b\bar{b}$: the Z, A and sbottom exchange all add up, and from the behavior of the non-negligible $A^A_{b\bar{b}}$ amplitude, we expect in region I an important total annihilation cross section $\sigma^A_{\chi-\chi}$ for high values of $\tan\beta$.

3.1.2 Region II

When m_0 increases ($<$ 1500–2000 GeV), m_A increases and, for intermediate $\tan\beta$ values, the $\chi\chi \xrightarrow{A} b\bar{b}$ amplitude decreases. Since sfermion masses also increase, the $\chi\chi \xrightarrow{\tilde{t}} t\bar{t}$ channel no longer cancels $\chi\chi \xrightarrow{Z} t\bar{t}$, which becomes the dominant process. However, for high $\tan\beta$, $\chi\chi \xrightarrow{A} b\bar{b}$ is enhanced and stays dominant. Globally, since all scalar masses have been increased by m_0, and the higgsino frac-

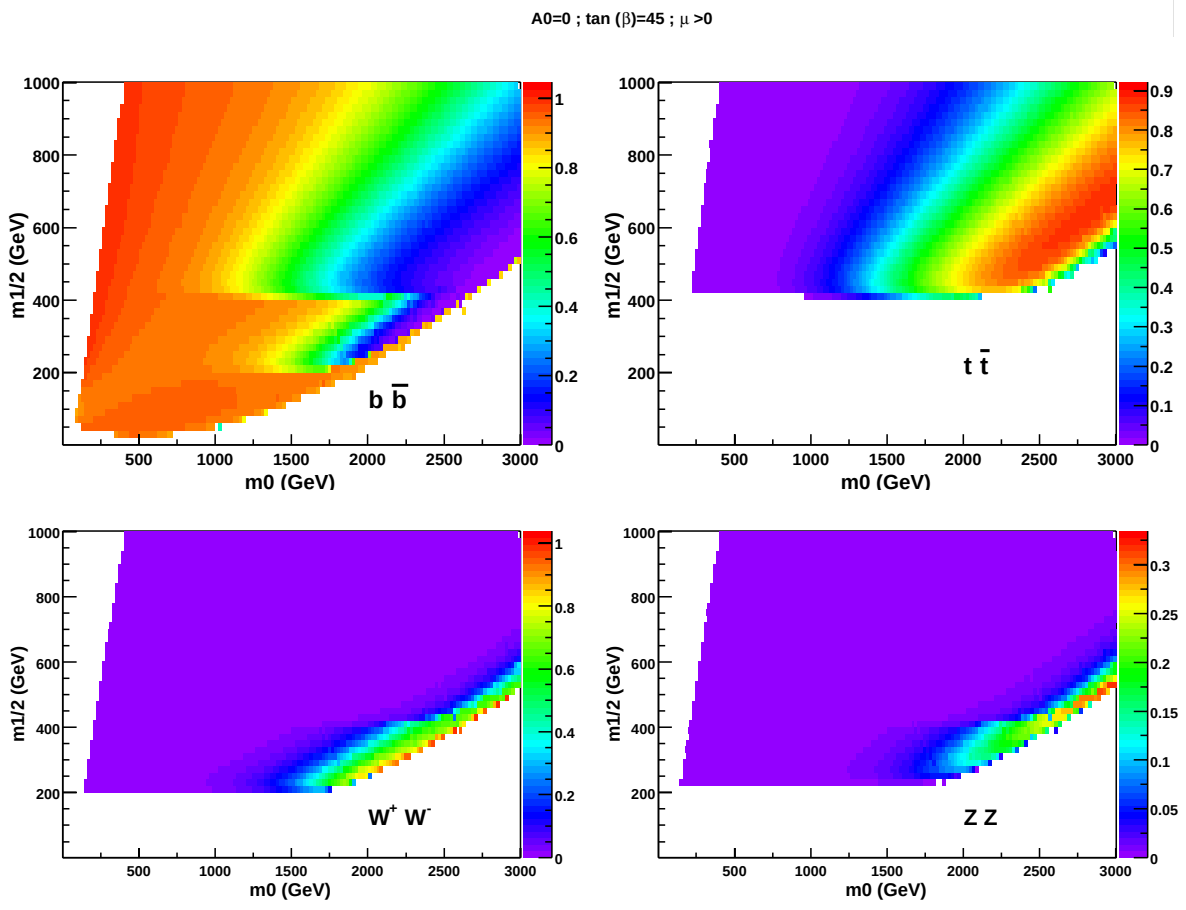

Fig. 4. Dominant branching ratios of the neutralino annihilation in the $(m_0, m_{1/2})$ plane

tion is still small, the neutralino annihilation cross section $\sigma^A_{\chi-\chi}$ is smaller than in region I.

3.1.3 Region III

Increasing further m_0 (> 2000–$2500\,\mathrm{GeV}$), for any value of $\tan\beta$, one finally approaches the mixed higgsino–bino region. The $\chi\chi \xrightarrow{Z} t\bar{t}$ channel amplitude $A^Z_{t\bar{t}} \propto (m_t m_\chi / m_Z^2)\, N^2_{3(4)}$ then dominates all other processes, which are suppressed by the increase of scalar masses. So we are left with a $t\bar{t}$ region parallel to the highest higgsino fraction isocurves. The m_0 value separating this region from the previous $\chi\chi \xrightarrow{A} b\bar{b}$ region depends on $\tan\beta$. All in all, the neutralino annihilation cross section $\sigma^A_{\chi-\chi}$ is strongly enhanced by Z exchange near the no-EWSB boundary.

3.2 Between top and W/Z thresholds

3.2.1 Region IV

Since $m_\chi < m_{\mathrm{top}}$, the neutralino annihilates almost only into $b\bar{b}$. Even if some $\chi\chi \xrightarrow{\tilde{b}} b\bar{b}$ occurs, the $\chi\chi \xrightarrow{A} b\bar{b}$ amplitude is dominant.

3.2.2 Region V

Increasing m_0 (and m_A), $\chi\chi \xrightarrow{A} b\bar{b}$ remains dominant and this process is still quite efficient for high values of $\tan\beta$. For intermediate values of $\tan\beta$, $\chi\chi \xrightarrow{A} b\bar{b}$ and $\chi\chi \xrightarrow{Z} b\bar{b}$ both occur, but their amplitudes are small and the total annihilation $\sigma^A_{\chi-\chi}$ is not efficient.

3.2.3 Region VI

Increasing further m_0 disfavors scalar exchange, but even though small, the higgsino fraction allows $\chi\chi \xrightarrow{\chi_i^+} W^+W^-$ and $\chi\chi \xrightarrow{\chi_i} ZZ$ to dominate and enhance the total annihilation cross section $\sigma^A_{\chi-\chi}$. Again, the m_0 values delimiting the boundary with region V depend on $\tan\beta$ (via m_A).

3.3 Below W/Z thresholds

3.3.1 Region VII

The dominant process is $\chi\chi \to b\bar{b}$ via A and/or Z exchange, depending on m_0, $\tan\beta$ and the higgsino fraction.

This analysis is illustrated on Figs. 4 and 13, showing the four most important branching ratios for $\tan\beta = 45$

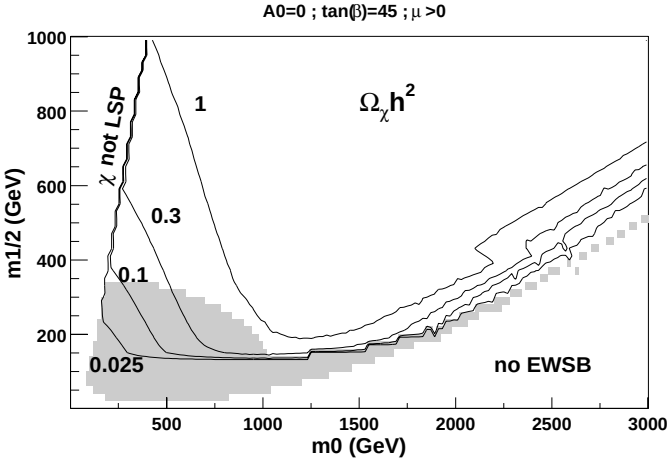

Fig. 5. Neutralino relic density in the $(m_0, m_{1/2})$ plane. A grey area indicates the excluded models by current accelerators constraints as discussed in the text

and 10 (the omitted process $\chi\chi \xrightarrow{A} \tau\bar{\tau}$ behaves as $\chi\chi \xrightarrow{A} b\bar{b}$ but with a smaller amplitude due to the m_τ/m_b ratio). It further offers a qualitative understanding of the relic density picture (Fig. 5). The annihilation is efficient for low values of m_0 (depending on $\tan\beta$) and for a mixed neutralino along the no-EWSB boundary. This gives the "V" (or "U") shape of the relic density profile for large (or small) $\tan\beta$. According to the current cosmological parameter values, we take the neutralino as an interesting cold dark matter candidate if $0.025 < \Omega h^2 < 0.3$. Figure 5 also shows the region in the $(m_0, m_{1/2})$ plane excluded by the experimental constraints from the Particle Data Group 2000 [26] implemented in DarkSUSY, that we have updated with: $m_{\chi_1^+} > 104\,\mathrm{GeV}$; $m_{\tilde{f}} > 100\,\mathrm{GeV}$ for $\tilde{f} = \tilde{t}_1, \tilde{b}_1, \tilde{l}^\pm, \tilde{\nu}$, $m_{\tilde{g}} > 300\,\mathrm{GeV}$; $m_{\tilde{q}_{1,2}} > 260\,\mathrm{GeV}$ for $\tilde{q} = \tilde{u}, \tilde{d}, \tilde{s}, \tilde{c}$ and $-6 \times 10^{-10} < a_\mu(\mathrm{SUSY}) < 58 \times 10^{-10}$ [27,28].

As noted in previous studies [29,17], the muon anomalous moment $a_\mu$and $b \to s\gamma$ branching ratio constraints strongly favor $\mu > 0$, to which we restrict ourselves in what follows. In Fig. 5, the grey tail at large m_0 is excluded by the chargino bound; it directly bites into the region relevant for neutrino indirect detection. Less relevant is the exclusion of small m_0 and $m_{1/2}$ values, which comes both from the Higgs mass limit and the $b \to s\gamma$ branching ratio, as calculated by default in DS. The range $\mathrm{BR}(b \to s\gamma) = 1 \to 4 \times 10^{-4}$ chosen by default in DarkSUSY may seem too low in view of latest CLEO and Belle measurements [26]. However the leading order calculation [30] implemented underestimates the SM value to 2.4×10^{-4}, while next to leading order corrections give 3.6×10^{-4} [31], so that this range should roughly correspond to $2.2 \to 5.2 \times 10^{-4}$, excluding a bit more than the range $2 \to 5 \times 10^{-4}$ chosen for instance in [17]. We have checked that replacing the implemented Higgs limit [32] by an aggressive version of the latest limit [33] ($m_h > 114\,\mathrm{GeV}$ for all $\sin(\beta - \alpha)$) only excludes a few more points around $(m_0 = 1000, m_{1/2} = 150)$, where neutrino fluxes are beyond reach.

In mSugra, $\chi\chi^+$ and $\chi\chi_2$ coannihilations (included in DS) occur only in the mixed neutralino region, decreasing further the relic density. $\chi\tilde{\tau}$ coannihilation occurs for low values of $\tan\beta$, for which there is no mixed region. $\chi\tilde{t}$ coannihilation [34,17,35] occurs for high values of A_0. In both cases, sfermion coannihilations (missing in DS) are relevant to lower the relic density in regions of large m_χ, which as we will see, are beyond the reach of indirect detection. We therefore do not expect their proper inclusion to change our conclusions.

4 Neutralino–proton cross section: Capture rate and direct detection signals

4.1 Capture

If present in the halo, relic neutralinos must accumulate in astrophysical bodies (of mass M_b) like the Sun or the Earth. The capture rate C depends on the neutralino–quark elastic cross section, $\sigma_{\chi-q}$. Neutralinos being Majorana particles, their vectorial interaction vanishes and the allowed interactions are scalar (via $\chi q \xrightarrow{H,h} \chi q$ in t-channel and $\chi q \xrightarrow{\tilde{q}} \chi q$ in s-channel) and axial (via $\chi q \xrightarrow{Z} \chi q$ in t-channel and $\chi q \xrightarrow{\tilde{q}} \chi q$ in s-channel). Depending on the spin content of the nuclei N present in the body, scalar and/or axial interactions are involved. Roughly, $C \sim (\rho_\chi / v_\chi) \sum_N M_b f_N(\sigma_N)/(m_\chi m_N)\langle v_{\mathrm{esc}}^2\rangle_N F(v_\chi, v_{\mathrm{esc}}, m_\chi, m_N)$, where ρ_χ, v_χ are the local neutralino density and velocity, f_N is the density of nucleus N in the body, σ_N the nucleus–neutralino elastic cross section, v_{esc} the escape velocity and F a suppression factor depending on the mismatching of masses and velocity. The neutralino capture is maximized for $m_\chi \sim m_N$ as $(\sigma_N)/(m_\chi m_N) \sim (m_r^2)/(m_\chi m_N) \doteq (m_\chi m_N)/((m_\chi + m_N)^2)$, and is much more efficient in the Sun than in the Earth as $M_\odot \gg M_\oplus$.

4.1.1 For the Earth

For the Earth, scalar interactions dominate. By increasing m_0 from its low value region, sfermions and H exchanges first decrease, and the cross section increases again when approaching the mixed higgsino region (see Fig. 6a). The capture rate is resonant for $m_\chi \sim 56\,\mathrm{GeV}$ around the iron mass.

4.1.2 For the Sun

For the Sun, the spin of hydrogen allows for axial interaction, which are stronger due to the Z coupling. The latter depends strongly on the neutralino higgsino fraction and is independent of $\tan\beta$, so the cross section follows the higgsino fraction isocurves as can be seen by comparing Figs. 6b and 1.

To summarize, due to the large solar mass and the spin dependent neutralino–quark cross section, the storage of neutralinos is much more efficient in the Sun than in the Earth.

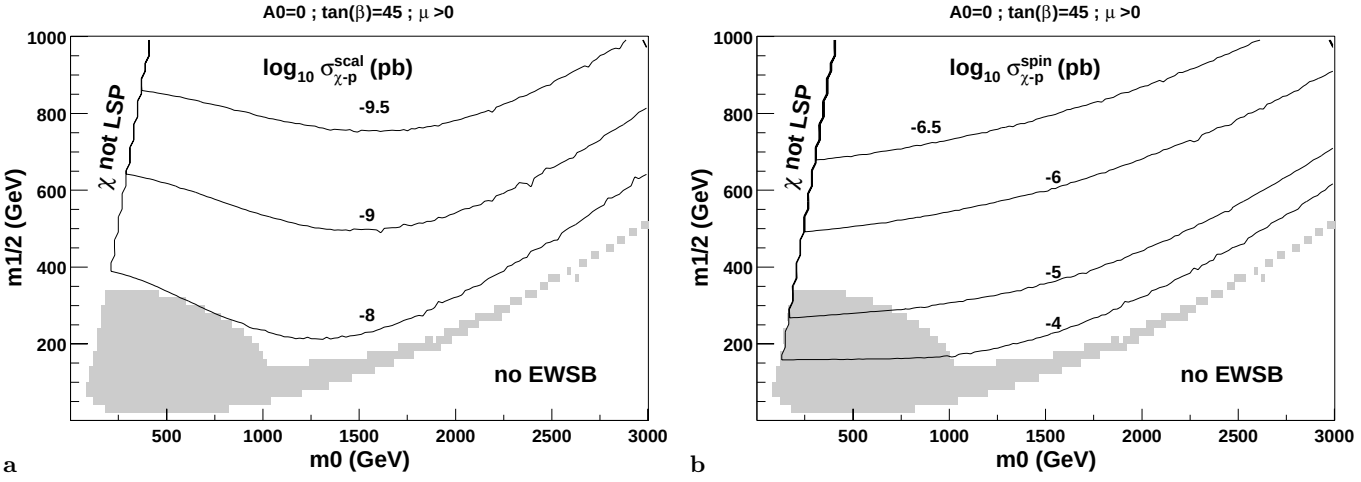

Fig. 6a,b. Scalar **a** and axial **b** cross sections for neutralino scattering on proton in pb

4.2 Direct detection

The elastic cross section of a neutralino on a nucleus also depends on $\sigma_{\chi-q}$, the nucleus mass number A and its spin content. Depending on the chosen nuclei target, current and future direct detection experiments are sensitive to the scalar coupling (CDMS (Ge) [36], Edelweiss (Ge) [37, 38], Zeplin (Xe) [39]) or to the axial coupling (MACHe3 (^{3}He) [40]). Comparison between experiment sensitivities and a set of mSugra models are shown on Fig. 9a.

5 Neutrino indirect detection

As $\chi\chi \to \nu\bar{\nu}$ is strongly suppressed by the tiny neutrino mass, neutrino fluxes come from decays of primary annihilation products, with a mean energy $E_\nu \sim m_\chi/2$ to $m_\chi/3$. The most energetic spectra, called "hard", come from neutralino annihilations into WW, ZZ and the less energetic, "soft" ones, come from $b\bar{b}$ [21]. Muon neutrinos give rise to muon fluxes by charged-current interactions in the Earth. As both the ν charged-current cross section on nuclei and the produced muon range are proportional to E_ν, high energy neutrinos are easier to detect. Considering that the population of captured neutralinos has a velocity below the escape velocity, and therefore neglecting evaporation, the number N_χ of neutralinos in the center of a massive astrophysical object depends on the balance between capture and annihilation rates: $\dot{N}_\chi = C - C_A N_\chi^2$, where C_A is the total annihilation cross section $\sigma^A_{\chi-\chi}$ times the relative velocity per volume. The annihilation rate at a given time t is then

$$\Gamma_A = \frac{1}{2} C_A N_\chi^2 = \frac{C}{2} \tanh^2 \sqrt{C C_A}\, t, \qquad (5)$$

with $\Gamma_A \approx C/2 = cste$ when the neutralino population has reached equilibrium, and $\Gamma_A \approx (1/2) C^2 C_A t^2$ in the initial collection period (relevant in the Earth). So, when accretion is efficient, the annihilation rate does not depend on annihilation processes, but follows the capture rate C and thus the neutralino–quark elastic cross section.

5.0.1 For the Sun

For the Sun, neutralinos do not reach complete equilibrium in the whole $(m_0, m_{1/2})$ plane studied, which contrasts with [29] based on Neutdriver [8] and different RGEs, probably yielding lighter (pseudo-)scalars and a lower μ. We find that the annihilation is on average less efficient (as attested to by our smaller region with an acceptable relic density), which results in a filling fraction $(CC_A)^{1/2} t_\odot$ smaller by a factor of 10 to 100. This has little effect on $\nu(\mu)$ fluxes for high m_0 or small $m_{1/2} <$ 600 GeV values, as equilibrium is nevertheless reached and fluxes follow essentially the higgsino fraction and the spin dependent $\sigma^{\rm spin}_{\chi-p}$ isocurves of Figs. 1a and 6. For low m_0 however, the equilibrium fluxes would drop with m_0 and C, but the smaller capture rate hinders equilibrium (e.g. $(CC_A)^{1/2} t_\odot \sim 1$ for $m_0 = 500$, $m_{1/2} = 800$), and Γ_A feels the increasing annihilation cross section. This effect is stronger for high $m_{1/2}$ values where the neutralinos are heavier and more bino-like, and where capture is smaller. The effect is also larger when $\tan\beta$ (and thus $\sigma^A_{\chi-\chi}$) is low, as incomplete equilibrium makes $\nu(\mu)$ fluxes sensitive to $\sigma^A_{\chi-\chi}$, making the W and top thresholds more conspicuous.

5.0.2 For the Earth

For the Earth, neutralinos are not in equilibrium. Neutrino fluxes depend both on C^2 and annihilation, giving an enhancement in the low and high m_0 regions where fluxes are boosted by annihilation (see Figs. 6 and 8). Since $M_\oplus < M_\odot$ and $\sigma^{\rm scal}_{\chi-p} < \sigma^{\rm spin}_{\chi-p}$, the capture rate and ν fluxes from the Earth are much smaller than from the Sun.

5.0.3 Comparing ν fluxes and μ fluxes

The $\nu \to \mu$ conversion factor increases with $m_{1/2}$ due to the increase of m_χ leading to more energetic neutrinos.

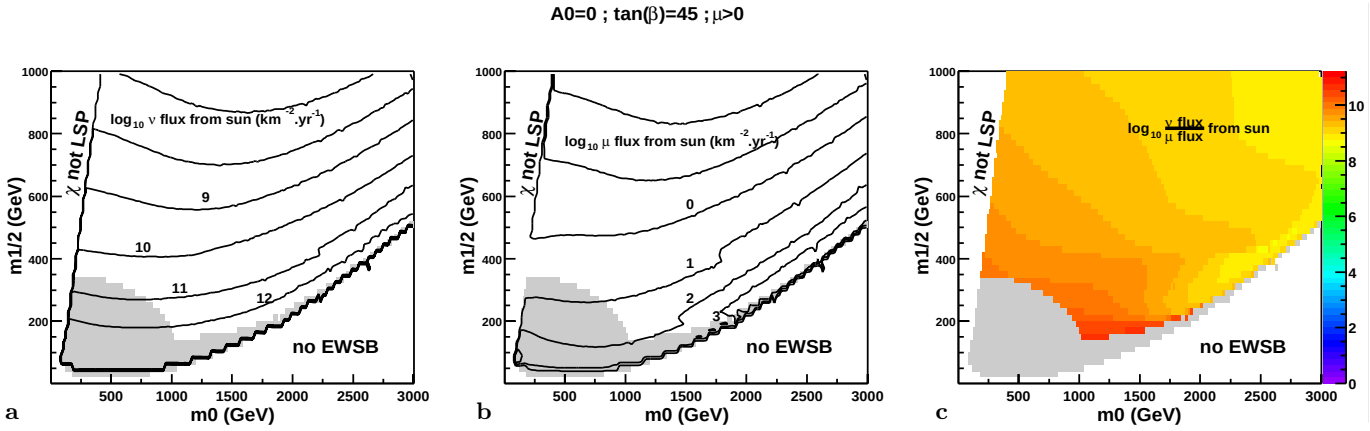

Fig. 7a–c. ν fluxes from the Sun **a**, the corresponding μ fluxes with $E_\mu > 5\,\mathrm{GeV}$ theshold **b** and their ratio **c**

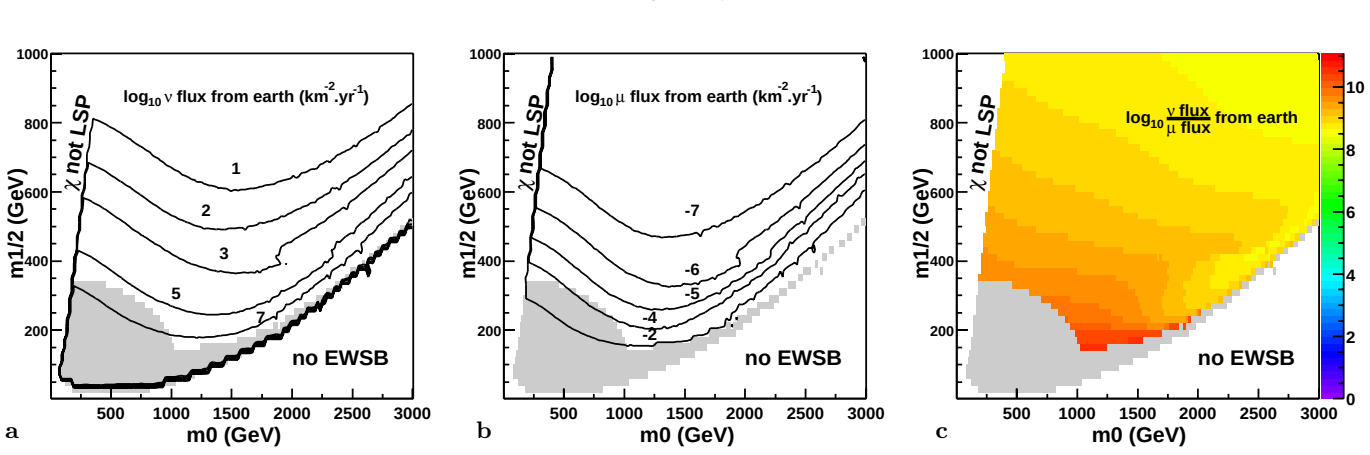

Fig. 8a–c. ν fluxes from the Earth **a**, the corresponding μ fluxes $E_\mu > 5\,\mathrm{GeV}$ theshold **b** and their ratio **c**

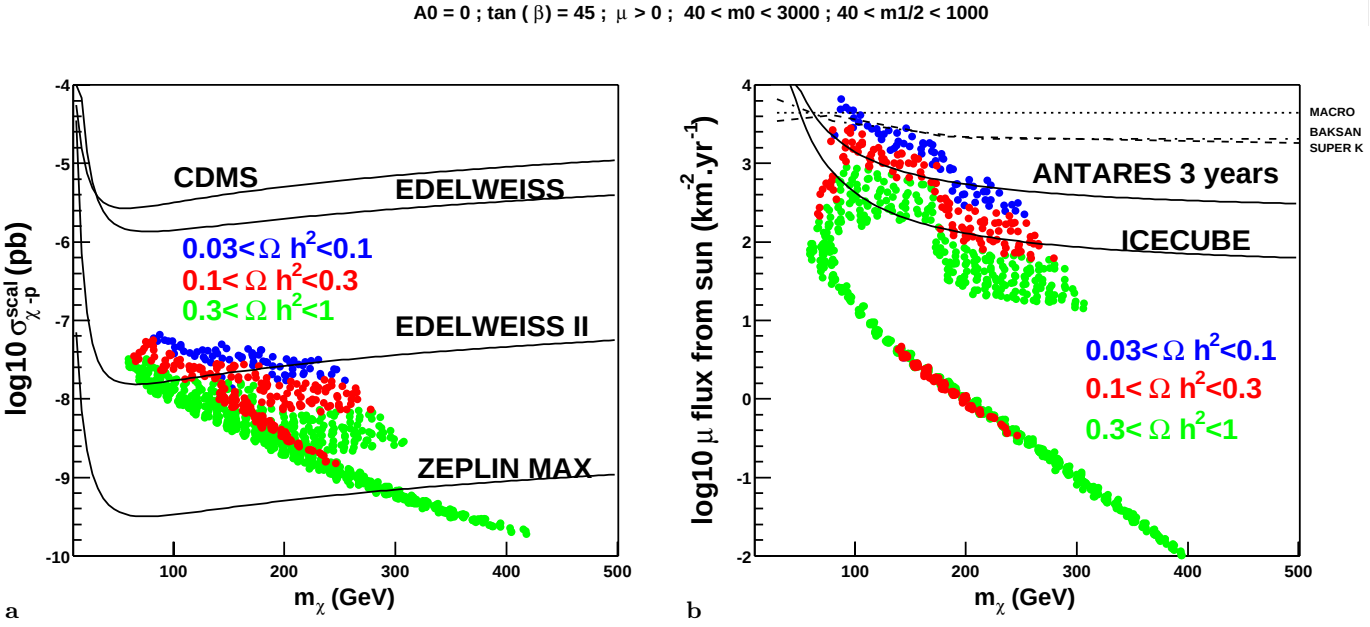

Fig. 9. **a** Direct detection experiment sensitivities and a set of models in the $(\sigma^{\mathrm{scal}}_{\chi-p}, m_\chi)$ plane. The models excluded by current accelerators constraints are not displayed. **b** Indirect detection experiment sensitivities in the $(\mu\mathrm{flux}_\odot, m_\chi)$ plane with $E_\mu = 5\,\mathrm{GeV}$ threshold of the same sample as **a**. Dotted, dash-dotted and dashed curves are respectively the Macro, Baksan and Super-Kamiokande upper limits. Solid lines indicate the future Antares and Icecube sensitivities

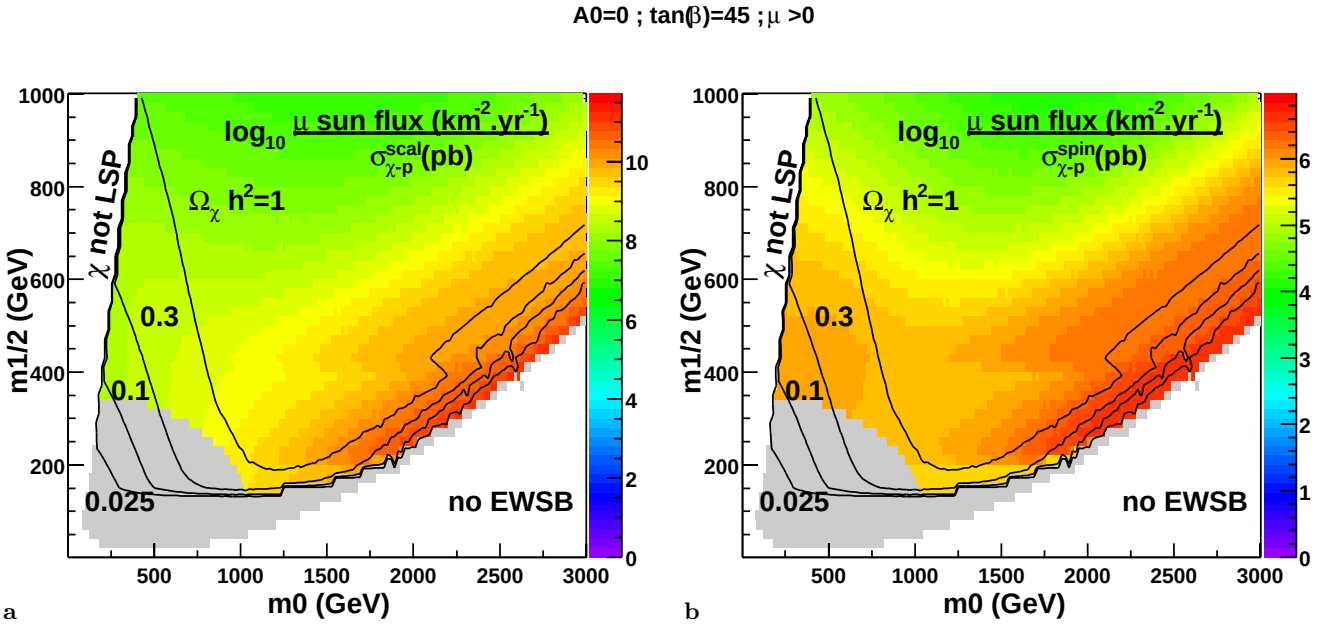

Fig. 10a,b. Comparison between μ fluxes from the Sun and neutralino–proton cross sections: **a** scalar, **b** spin dependent

This ratio also follows the annihilation final state regions described in Sect. 3 above. Indeed, the spectra from WW, ZZ and to a lesser extent $t\bar{t}$ are more energetic than the $b\bar{b}$ spectra, so neutrino conversion into the muon is more efficient in the mixed bino–higgsino region above W and top thresholds (see Figs. 7 and 8).

5.0.4 Comparison with indirect detection experiment sensitivities

Muon fluxes coming from neutralino annihilation in the Sun are shown in Fig. 9b. MSugra models predicting a good relic density of neutralinos give neutrino/muon fluxes which can be as high as the current experimental limits (Baksan [41], Macro [42], Super Kamiokande [43]). The 0.1 km^2 Antares detector will explore further the interesting parameter space [44]. Next generation neutrinos telescopes (Icecube, Antares km^3) will be much more efficient to test such models, e.g. the Icecube expected sensitivity is $\sim 10^2 \mu\,\mathrm{km}^2\,\mathrm{yr}^{-1}$ from the Sun [45].

5.0.5 Indirect versus direct detection

A high neutralino–proton cross section is efficient in both direct and indirect detection (via capture). The large m_0 mixed higgsino–bino region pointed out in [15,29] favors both direct and indirect detection due to the enhancement of $\sigma_{\chi-p}$ and $\sigma^A_{\chi-\chi}$. Both enter in the indirect detection which is moreover favored by the production of more energetic neutrinos in WW, ZZ and $t\bar{t}$ decays, leading to better conversion into muons (Fig. 10). This mixed region, which has a good relic density, is very attractive for neutrino indirect detection signal.

Hovewer, no current experiment is able to really test such models. Figure 11 shows the region of the $(m_0, m_{1/2})$ plane which can be explored by future direct detection experiments and neutrino telescopes.

6 Variations

In this section, we discuss the robustness of the indirect detection picture described above, with respect to variations in SUSPECT 2.002 of

(1) mSugra input parameters like A_0 or $\tan\beta$,
(2) experimental uncertainties on the top quark mass and
(3) theoretical uncertainties on the scale of electroweak symmetry breaking Q_{EWSB}

6.1 A_0

Varying A_0 away from 0 does not change too much the analysis above. Annihilation branching ratio regions, as well as the no-EWSB boundary and slope can be slightly displaced. For moderate $\tan\beta \sim 20$, quite large and negative values of A_0 (e.g. -800 GeV) can enhance the $\tau^+\tau^-$ annihilation channel along the $\tilde{\tau}$ LSP region (i.e. low m_0) due to splitting in the $\tilde{\tau}$ mass matrix. For such values, the $\tilde{\tau}\chi$ coannihilation [46] could also affect the relic density, but in this region, neutrino fluxes are too small to be detected anyway (see Fig. 12). The same happens with the $t\bar{t}$-channel for $400 < m_{1/2} < 600$ and $m_0 < 700$ ($\sim |A_0|$). The $\tilde{t}\chi$ [34,17,35] coannihilation can also occur for $A_0 \sim -2000$ GeV, but the usual cosmologically interesting region is reduced (due to the negative squared mass arising in sfermion matrices at low m_0 and because the mixed region is pushed to higher values of m_0). In addition, this coannihilation region produces neutrino fluxes from the Sun around $10^{-1}\mu\,\mathrm{km}^{-2}\,\mathrm{yr}^{-1}$, too low to be detected. In view of the latest results on cosmological parameters, Fig. 12a shows models with $0.03 < \Omega h^2 < 0.3$ in

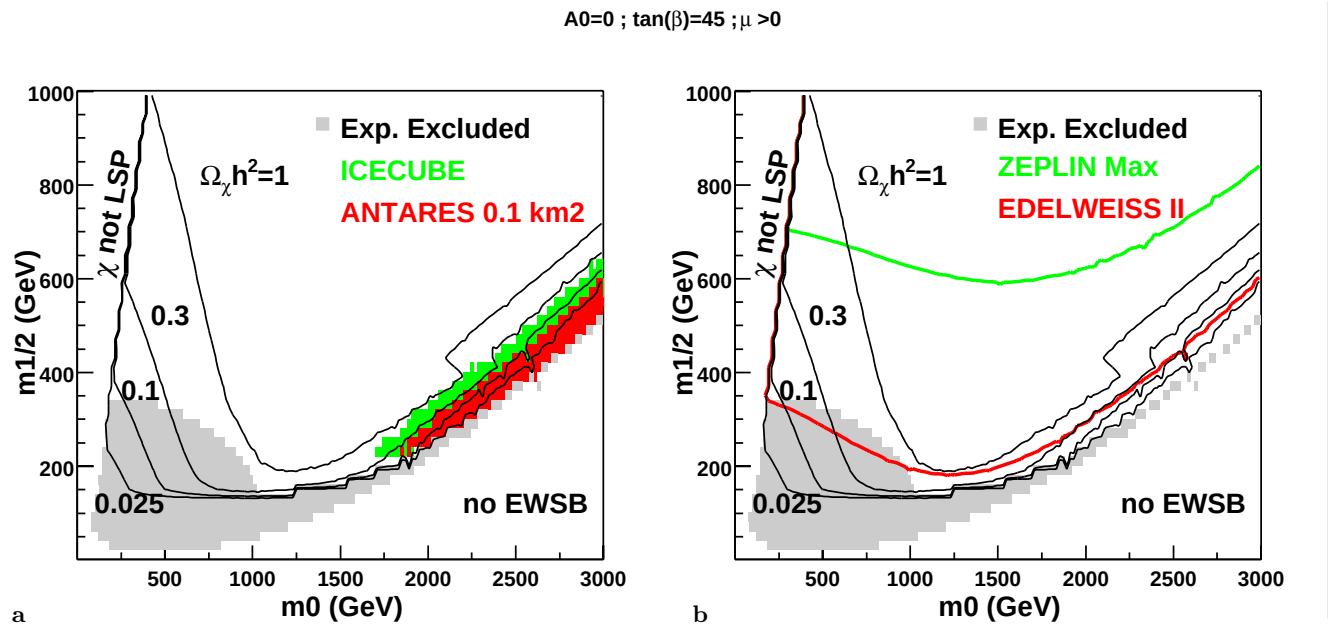

Fig. 11. **a** ν telescopes' sensitivities on μ fluxes from the Sun and **b** direct detection experiments' sensitivities in the $(m_0, m_{1/2})$ plane

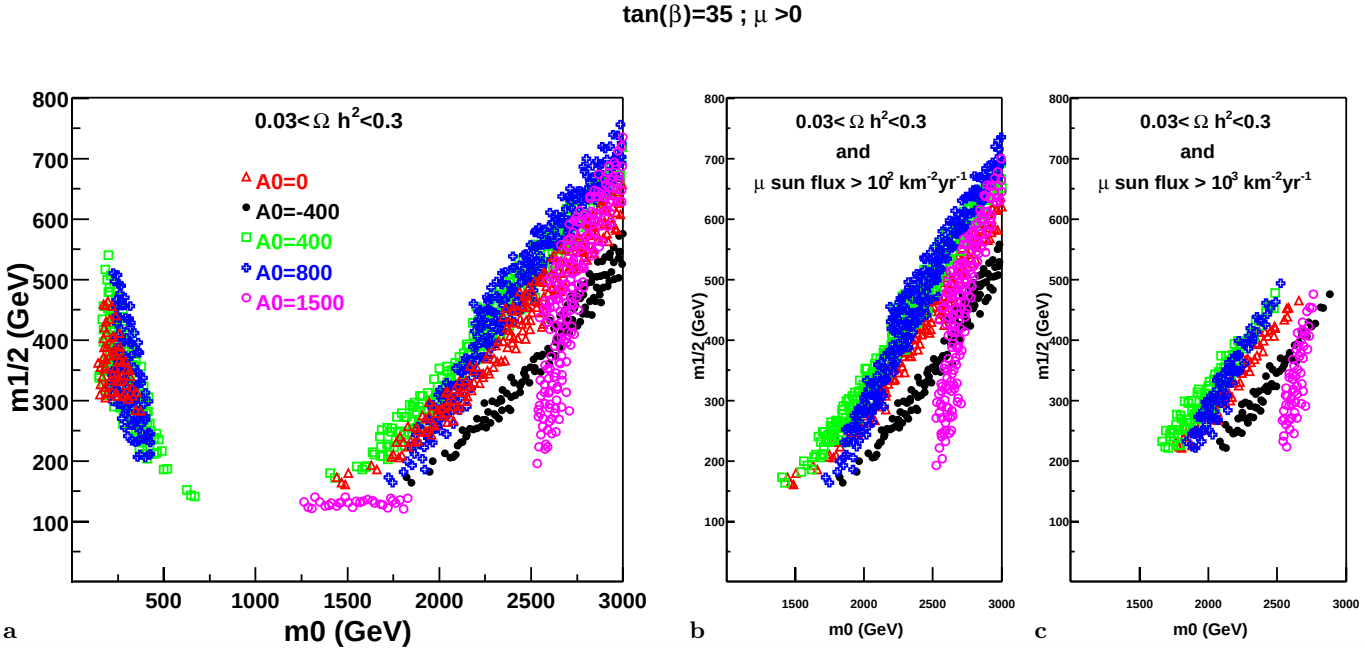

Fig. 12. **a** Cosmologically favored models for different values of A_0 in the $(m_0, m_{1/2})$ plane; a subset of these models generating a μ flux from the Sun larger than **b** $10^2\,\mathrm{km}^{-2}\,\mathrm{yr}^{-1}$; **c** $10^3\,\mathrm{km}^{-2}\,\mathrm{yr}^{-1}$

the $(m_0, m_{1/2})$ plane for different values of A_0, as well as models giving μ fluxes from the Sun larger than 10^2 (b) and $10^3 \mu\,\mathrm{km}^{-2}\,\mathrm{yr}^{-1}$ (c). The latter models are confined in the mixed higgsino–bino region. In addition, only those models with $m_W < m_\chi < m_t$ giving a hard spectrum of neutrinos via $\chi\chi \xrightarrow{\chi_i^+} W^+W^-$ and $\chi\chi \xrightarrow{\chi_i} ZZ$ can simultaneously satisfy $0.1 < \Omega h^2 < 0.3$, while yielding a high muon flux.

6.2 tan β

The branching ratio picture does not qualitatively change for different values of $\tan\beta$. Low values of $\tan\beta$ can add a $\chi\chi \to t\bar{t}$ region for low m_0 and open a $\tilde{\tau}\chi$ coannihilation [46] region along the $\tilde{\tau}$ LSP region, but μ fluxes are small and such values of $\tan\beta$ reduce the mixed neutralino region which is the most interesting for indirect detection. As discussed previously, the boundaries of the branching

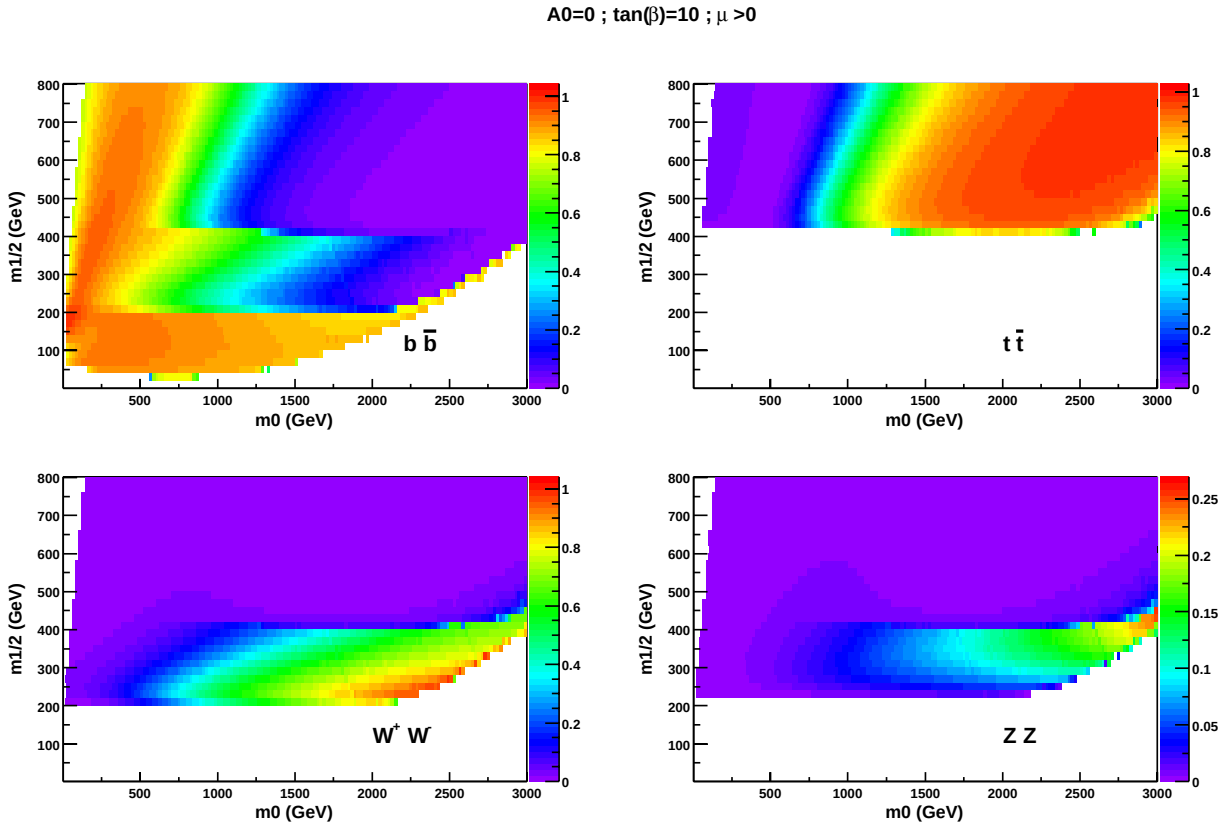

Fig. 13. Branching ratio of the neutralino annihilation in the $(m_0, m_{1/2})$ plane (same as Fig. 4 for $\tan\beta = 10$)

ratio regions move with $\tan\beta$ (compare Figs. 13 and 4). When $\tan\beta$ grows, the cosmologically motivated region is wider due to the annihilation enhancement via A exchange (in regions I/II and IV/V). Applying the conservative cut $0.03 < \Omega h^2 < 0.3$, all values of $\tan\beta$ provide interesting models for neutrino indirect detection (see Fig. 14). For too large values of $\tan\beta$, the $b\bar{b}$ region is extended and leads to soft neutrino spectra. In this case it becomes more difficult to reconciliate a tighter limit on the relic density with current experimental sensitivities. Values of $\tan\beta \sim 10 \to 35$ give more models satisfying both relic density $0.1 < \Omega h^2 < 0.3$ and high ν/μ fluxes.

6.3 EWSB scale

$Q_{\rm EWSB}$ is the scale at which the running of the soft SUSY breaking terms is frozen and the minimization of the scalar potential is achieved. When the full potential is minimized within a multi-scale RG treatment, $Q_{\rm EWSB}$ should not affect the physics. Hovewer, the one-loop single scale effective potential does depend on $Q_{\rm EWSB}$, and the tree-level relations ((4)) only hold in terms of running parameters at $Q_{\rm EWSB}$; if $Q_{\rm EWSB}$ is chosen $\sim (m_{\tilde{t}_1} m_{\tilde{t}_2})^{1/2}$ [13], the potential can be minimized pertubatively. Varying $Q_{\rm EWSB}$ away from this value is therefore not physical, but gives a hint on the theoretical uncertainties associated with a single scale RG and potential minimization approach. When $Q_{\rm EWSB}$ is lowered, the RG running drives μ to smaller values. This leads to a wider region of the $(m_0, m_{1/2})$ plane where EWSB cannot be achieved. In the remaining allowed region, the lower values of μ slightly increases the higgsino fraction of the neutralino and the annihilation cross section, giving more cosmologically acceptable models. Figures 15 and 16 show the relic density and μ fluxes from the Sun and the Earth in the $(m_0, m_{1/2})$ plane for $Q_{\rm EWSB} = (1/2)(m_{\tilde{t}_1} m_{\tilde{t}_1})^{1/2}$ and $(1/5)(m_{\tilde{t}_1} m_{\tilde{t}_1})^{1/2}$. For $Q_{\rm EWSB} = (1/5)(m_{\tilde{t}_1} m_{\tilde{t}_2})^{1/2}$, one sees around $m_0 = m_{1/2}$ the $\chi\chi \xrightarrow{A} b\bar{b}$ s-channel annihilation pole which would otherwise show up for higher values of $\tan\beta \gtrsim 55$ [17]. It affects significantly the fluxes from the Earth, where capture and annihilation are not in equilibrium; see Fig. 16c. The higher higgsino fraction also enhances the elastic cross section $\sigma_{\chi-q}$, but the stronger annihilation reduces the number of models which are both interesting from the cosmological point of view and in terms of Sun muon fluxes (Fig. 19c). As before, muon fluxes from the Earth are much too weak to be detected. An increasing $Q_{\rm EWSB}$ leads to the opposite effect: higher values of $|\mu|$ and a reduced cosmological favored region.

6.4 Top mass

The current experimental value is $m_t = 174.3 \pm 5.1\,\text{GeV}$ [26]. Our default choice up to now has been to adopt the central value. Lowering m_t implies that the top Yukawa coupling Y_t is smaller so that the RG decreasing of $m^2_{H_u}$ is

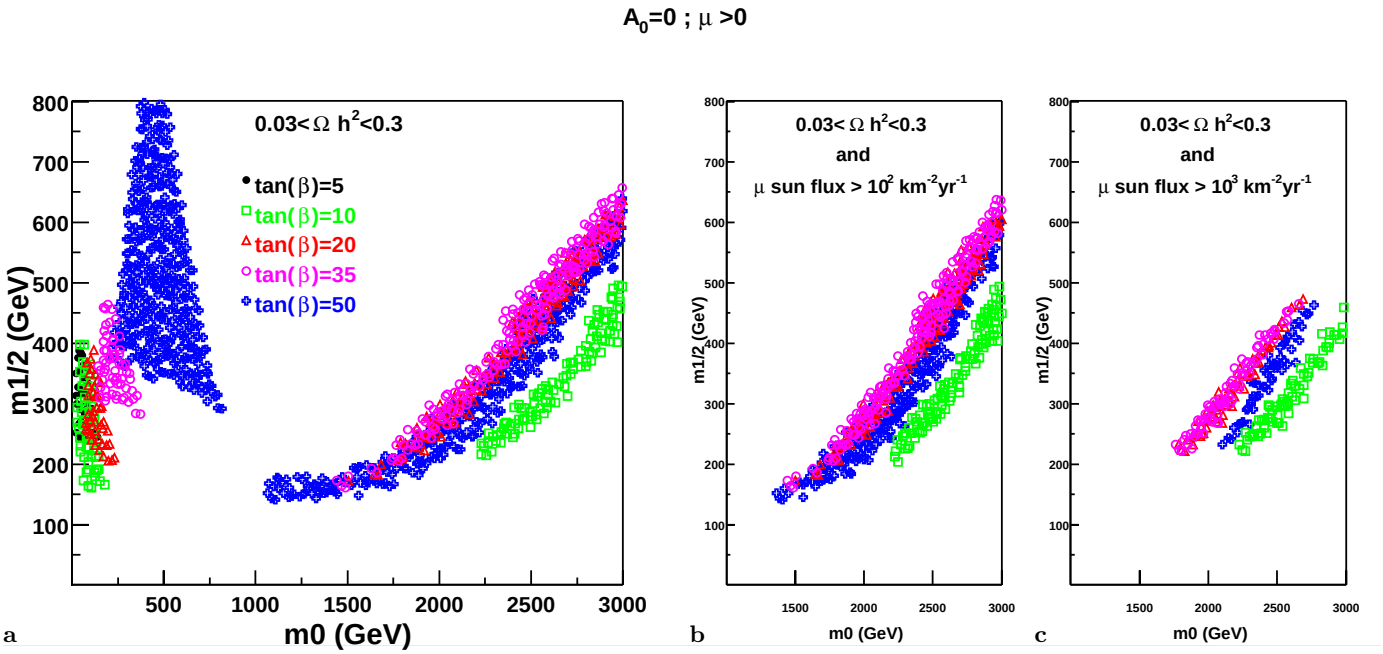

Fig. 14. **a** Cosmologically favored models for differents values of $\tan\beta$ in the $(m_0, m_{1/2})$ plane; a subset of these models generating a μ flux from the Sun larger than **b** $10^2\,\mathrm{km}^{-2}\,\mathrm{yr}^{-1}$; **c** $10^3\,\mathrm{km}^{-2}\,\mathrm{yr}^{-1}$

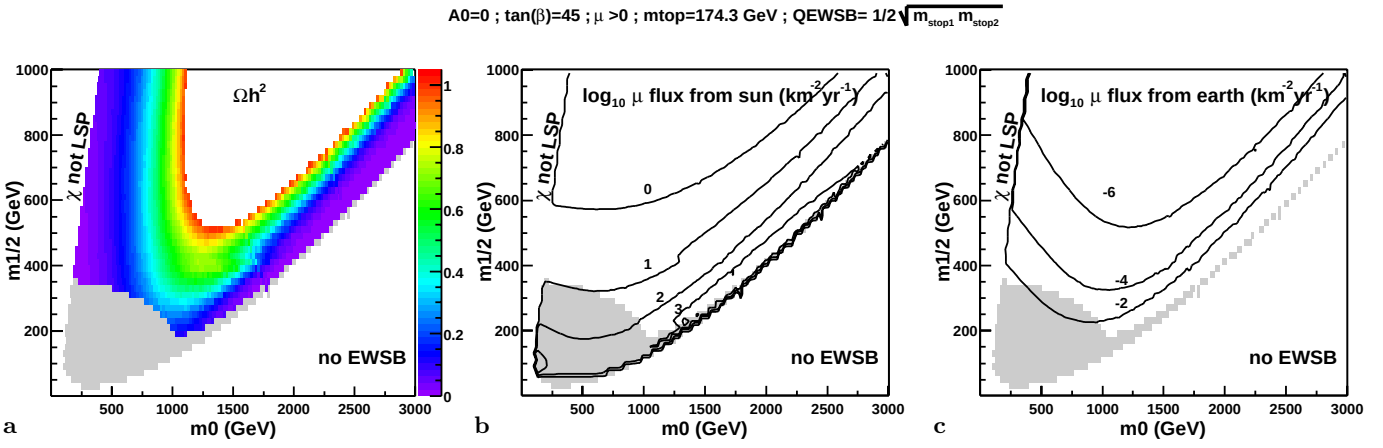

Fig. 15. **a** Relic density, μ fluxes from the Sun **b** and the Earth **c** in the $(m_0, m_{1/2})$ plane for $Q_{\mathrm{EWSB}} = (1/2)(m_{\tilde{t}_1} m_{\tilde{t}_2})^{1/2}$ and $m_t = 174.3\,\mathrm{GeV}$

less efficient and the region where EWSB does not occur is wider (see (4), and Figs. 17 and 18). Nevertheless the mixed higgsino region is larger favoring annihilation and capture, but there are no additional models combining a large ν/μ flux with an acceptable relic density (Figs. 17, 18 and 19). Increasing the top mass leads to the opposite effect, which is less interesting for our study. It should also be noticed that varying Q_{EWSB} and/or m_t allows for heavier neutralino within the fixed Ωh^2 interval.

7 Conclusion

In this paper, we have analyzed, within the framework of the constrained minimal supersymmetric standard model (a.k.a. mSugra), the possible indirect detection of neutralino dark matter through the neutrinos produced by its annihilation in the Earth and the Sun. In particular, we have presented an original study of the relative weight of various annihilation channels crucial to indirect detection. Fixing the halo dark matter density to $\rho_\chi = 0.3\,\mathrm{GeV/cm}^3$ and allowing for the widest range of cosmological relic density $0.03 < \Omega h^2 < 0.3$, we find that a neutrino signal from the center of the Earth is beyond reach of the present and even future neutrino telescopes.

For the larger Sun, we find that a neutrino signal may be found, but only in the large m_0 "focus point" region [15, 29] where the neutralino has a larger higgsino component which increases both neutralino–nucleon elastic scattering and neutralino annihilation cross sections. Since in this re-

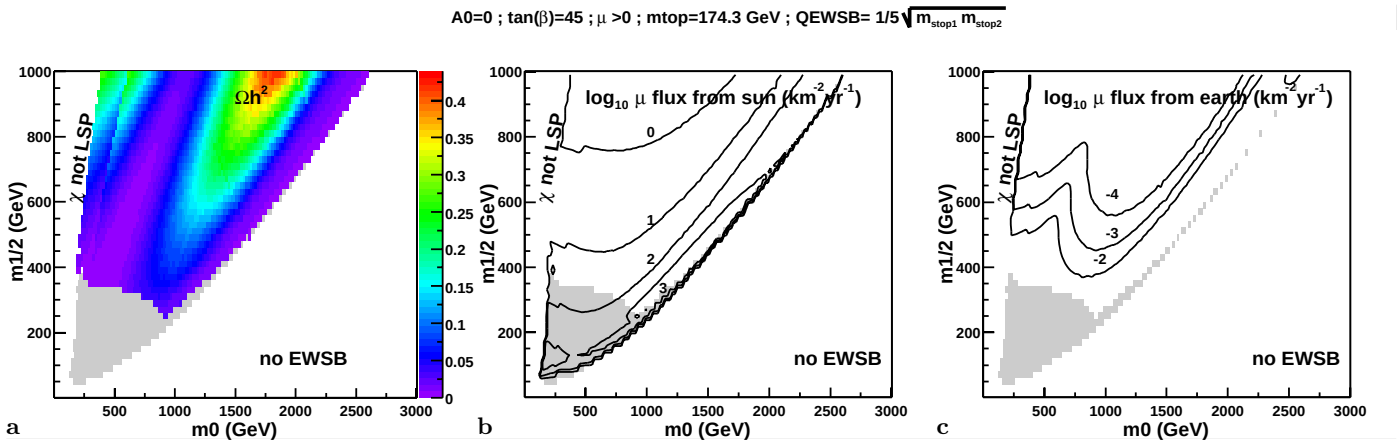

Fig. 16. **a** Relic density, μ fluxes from the Sun **b** and the Earth **c** in the $(m_0, m_{1/2})$ plane for $Q_{\rm EWSB} = (1/5)(m_{\tilde{t}_1} m_{\tilde{t}_2})^{1/2}$ and $m_t = 174.3\,{\rm GeV}$

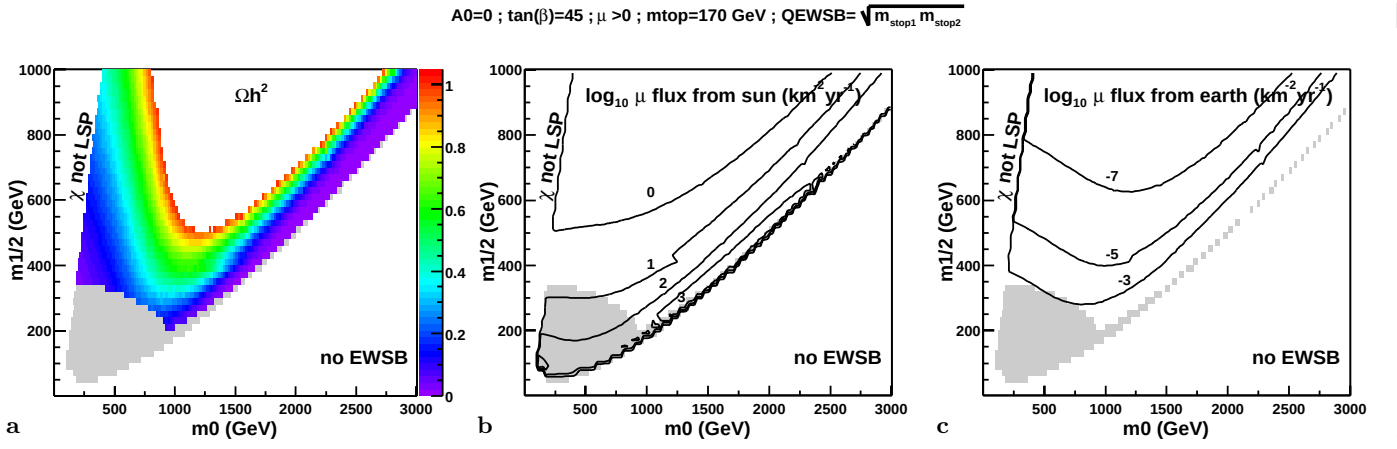

Fig. 17. **a** Relic density, μ fluxes from the Sun **b** and the Earth **c** in the $(m_0, m_{1/2})$ plane for $Q_{\rm EWSB} = (m_{\tilde{t}_1} m_{\tilde{t}_2})^{1/2}$ and $m_t = 170\,{\rm GeV}$

gion, both are related by s- and t-channel crossing (exactly above $t\bar{t}$ threshold and approximately below), any parameter change reducing the relic density inevitably increases the neutrino flux. When conversion into muons is taken into account with a 5 GeV threshold on the muon energy, the only models providing both a relevant (but rather low) relic density, and fluxes around the *current* indirect detection sensitivity ($10^3 \mu{\rm km}^{-2}\,{\rm yr}^{-1}$) are those with $m_\chi < m_t$ and $\chi\chi \xrightarrow{\chi_i^+} W^+W^-$ or $\chi\chi \xrightarrow{\chi_i} ZZ$ as dominant annihilation processes. Relaxing the tight mSugra constraints in specific directions could favor such channels [47]. The next generation of neutrino telescopes (with a km^3 size) will be much more efficient to probe mSugra models, especially for $m_\chi > m_t$. If a neutrino signal is found in this framework, then neutralino dark matter should also be accessible to future direct detection experiments, and a chargino with $m_{\chi^+} < 350\,{\rm GeV}$ should be found in accelerators.

To conclude, a comparison with previous related work is in order. Earlier studies [8,48] of neutralino indirect detection were performed in the unconstrained MSSM, where μ is a free parameter, and mixed neutralinos occur rather easily. Taking an mSugra slice in this huge parameter space obviously introduces many correlations, for instance between the neutrino flux and the relic density or $\sigma^{\rm spin}_{\chi-p}$ (and even $\sigma^{\rm scal}_{\chi-p}$). The effect of this slicing in the $(m_\chi, \sigma^{\rm scal}_{\chi-p})$ plane was shown in [49] for small $\tan\beta$ and in [50] for large $\tan\beta$. Our Fig. 9 agrees with this last result, with the addition of the focus point region forming the upper-right cloud. We should note however that a comparison in the $(m_0, m_{1/2})$ plane is more difficult, specially at large $\tan\beta$, because of the theoretical uncertainties in the RGE used to translate these parameters into physical quantities. As an example, for a given value of $\tan\beta$, the slope of the EWSB boundary decreases between [29], this work and [50]. As another example, strong annihilation via s-channel A, H_0 scalars appears above $\tan\beta > 50$ in [51,52], $\tan\beta > 35$ in [50], and $\tan\beta > 60$ (or $\tan\beta = 45$, $Q_{\rm EWSB} = (m_{\tilde{t}_1} m_{\tilde{t}_2})^{1/2}/5$, see Fig. 16) in the present work using SUSPECT. Finally, we find a muon event rate compatible with [29], and larger than [51]. Part of this difference comes from a higher threshold (25 GeV instead of our 5 GeV). The rest might be attributed to a high sensitivity in the renormalization group equations at large m_0 and $\tan\beta$. It seems [24] that using SOFTSUSY [25] or SUS-

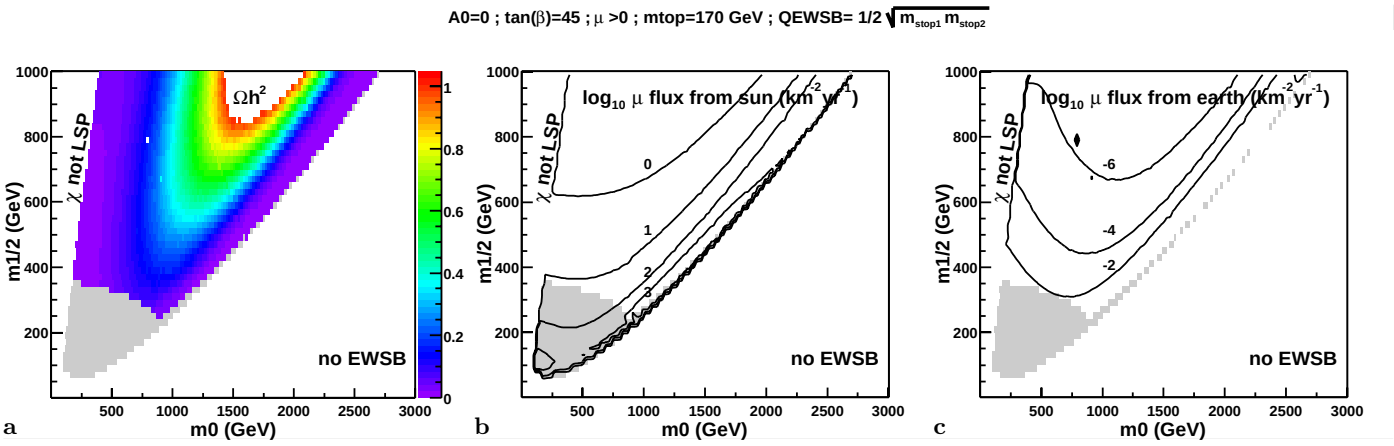

Fig. 18. **a** Relic density, μ fluxes from the Sun **b** and the Earth **c** in the $(m_0, m_{1/2})$ plane for $Q_{\rm EWSB} = (1/2)(m_{\tilde{t}_1} m_{\tilde{t}_2})^{1/2}$ for $m_t = 170\,{\rm GeV}$

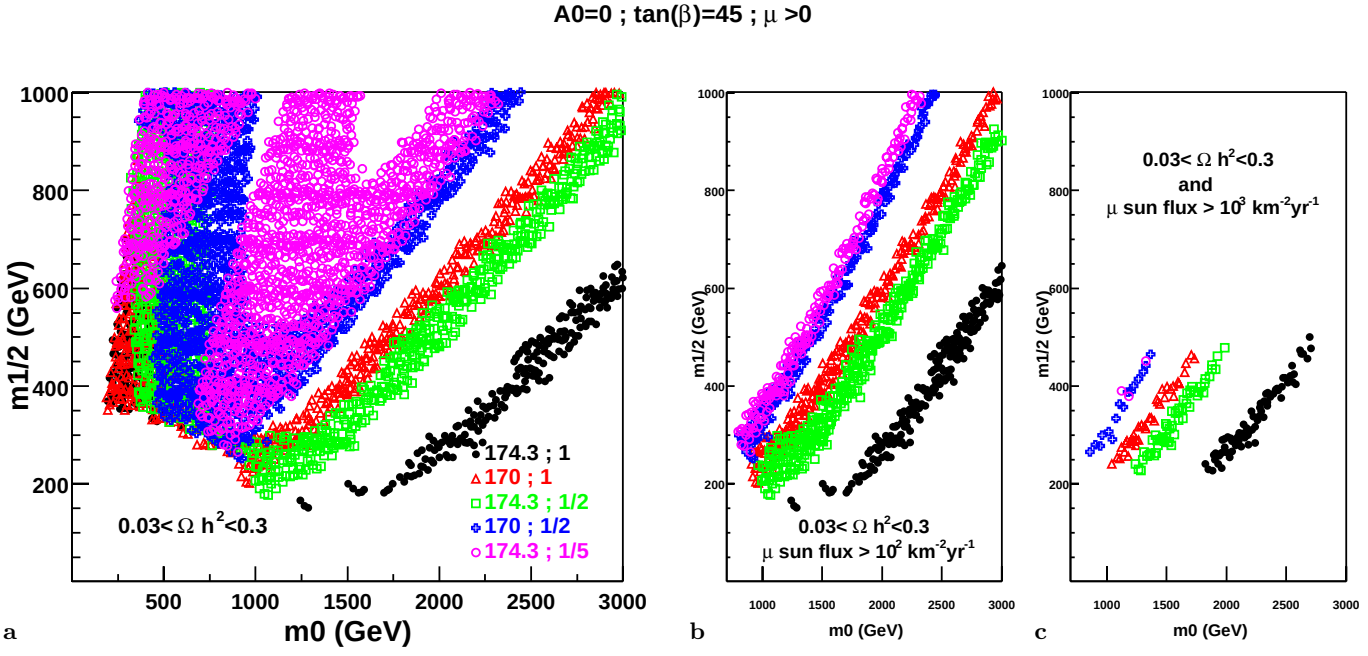

Fig. 19. **a** Dark matter favored models for different values of $Q_{\rm EWSB}$ and top mass in the $(m_0, m_{1/2})$ plane **a**. Colors and symbols correspond to different values of m_t and $Q_{\rm EWSB}$: e.g. (170; 1/2) means $m_t = 170\,{\rm GeV}$ and $Q_{\rm EWSB} = (1/2)(m_{\tilde{t}_1} m_{\tilde{t}_2})^{1/2}$. The models that moreover yield a muon flux from the Sun larger than $> 10^2\,{\rm km}^{-2}\,{\rm yr}^{-1}$ and $> 10^3\ {\rm km}^{-2}\,{\rm yr}^{-1}$ are shown in **b** and **c**

PECT [16,17] may be safer than ISASUGRA [53] in this region.

Acknowledgements. This work would not have started without the French "GDR supersymetrie". We gratefully thank Jean-Loic Kneur, Charling Tao, and the Antares Neutralino WG for help and stimulating discussions. We must also underline the acute reading and very constructive role of the referee in the final version of this article.

References

1. J.A. Peacock, Cosmological physics, chapter 3 (Cambridge University Press 1999)
2. C.H. Lineweaver, Cosmological parameters. 2001, talk presented at COSMO-01, Rovaniemi, Finland August 29–September 4
3. P. Fayet, S. Ferrara, Phys. Rept. **32**, 249 (1977)
4. R. Barbieri, Riv. Nuovo Cim. **11**, 1 (1988)
5. S.P. Martin, A supersymmetry primer. Perspectives on Supersymmetry. Advanced Series on Directions in High Energy Physics, Vol. 18 (World Scientific, 1998)
6. J.A. Bagger, Weak-scale supersymmetry: Theory and practice, Proceedings of the Boulder 1995 TASI Lectures (QCD161:T45:1995)
7. H.E. Haber, G.L. Kane, Phys. Rept. **117**, 75 (1985)
8. G. Jungman, M. Kamionkowski, K. Griest, Phys. Rept. **267**, 195 (1996)
9. H.P. Nilles, Phys. Rept. **110**, 1 (1984)

10. A.H. Chamseddine, R. Arnowitt, P. Nath, Phys. Rev. Lett. **49**, 970 (1982)
11. R. Barbieri, S. Ferrara, C.A. Savoy, Phys. Lett. B **119**, 343 (1982)
12. L.J. Hall, J. Lykken, S. Weinberg, Phys. Rev. D **27**, 2359 (1983)
13. G. Gamberini, G. Ridolfi, F. Zwirner, Nucl. Phys. B **331**, 331 (1990)
14. J.L. Feng, K.T. Matchev, T. Moroi, Phys. Rev. D **61**, 075005 (2000)
15. J.L. Feng, K.T. Matchev, F. Wilczek, Phys. Lett. B **482**, 388 (2000)
16. A. Djouadi, J.L. Kneur, G. Moultaka, Suspect program, http://www.lpm.univ-montp2.fr:7082/kneur/suspect.html
17. A. Djouadi, M. Drees, J.L. Kneur, JHEP **08**, 055 (2001)
18. D.J. Castano, E.J. Piard, Pierre Ramond, Phys. Rev. D **49**, 4882 (1994)
19. V.D. Barger, M.S. Berger, P. Ohmann, Phys. Rev. D **49**, 4908 (1994)
20. Damien M. Pierce, Jonathan A. Bagger, Konstantin T. Matchev, Ren-jie Zhang, Nucl. Phys. B **491**, 3 (1997)
21. P. Gondolo, J. Edsjo, L. Bergstrom, P. Ullio, E.A. Baltz, Darksusy: A numerical package for dark matter calculations in the MSSM, astro-ph/0012234, Proceedings of York 2000, the identification of dark matter, pp. 318–323
22. P. Gondolo, J. Edsjo, L. Bergstrom, P. Ullio, T. Baltz, Darksusy program, http://www.physto.se/edsjo/darksusy/
23. T. Nihei, L. Roszkowski, R. Ruiz de Austri, JHEP **05**, 063 (2001)
24. B.C. Allanach, Theoretical uncertainties in sparticle mass predictions, hep-ph/0110227, submitted to aps / dpf / dpb summer study on the future of particle physics (Snowmass 2001), Snowmass, Colorado, 30 June–21 July 2001
25. B.C. Allanach, Comput. Phys. Commun. **143**, 305 (2002)
26. D.E. Groom et al., Review of particle physics. Eur. Phys. J. C **15**, 1 (2000)
27. Marc Knecht, Andreas Nyffeler, Phys. Rev. D **65**, 073034 (2002)
28. Andrzej Czarnecki, William J. Marciano, Phys. Rev. D **64**, 013014 (2001)
29. J.L. Feng, K.T. Matchev, F. Wilczek, Phys. Rev. D **63**, 045024 (2001)
30. S. Bertolini, F. Borzumati, A. Masiero, G. Ridolfi, Nucl. Phys. B **353**, 591 (1991)
31. M. Ciuchini, G. Degrassi, P. Gambino, G.F. Giudice, Nucl. Phys. B **527**, 21 (1998)
32. R. Barate et al., Eur. Phys. J. C **17**, 223 (2000)
33. A. Heister et al., Phys. Lett. B **526**, 191 (2002)
34. C. Boehm, A. Djouadi, M. Drees, Phys. Rev. D **62**, 035012 (2000)
35. J.R. Ellis, K.A. Olive, Y. Santoso, Calculations of neutralino stop coannihilation in the CMSSM, cern-th-2001-339, umn-th-2032-01, tpi-minn-01-50, hep-ph/0112113
36. R. Abusaidi et al., Phys. Rev. Lett. **84**, 5699 (2000)
37. A. Benoit et al., Improved exclusion limits from the Edelweiss WIMP search, astro-ph/0206271
38. G. Chardin, Edelweiss dark matter search, talk given at the school and workshop on neutrino particle astrophysics, Les Houches 21 January–1 February 2002
39. N. Spooner, New limits and progress from the boulby dark matter programme, talk given at the school and workshop on neutrino particle astrophysics, Les Houches 21 January–1 February 2002
40. F. Mayet, D. Santos, Yu.M. Bunkov, E. Collin, H. Godfrin, Phys. Lett. B **538**, 257 (2002)
41. Olga V. Suvorova, Status and perspectives of indirect search for dark matter, published in Tegernsee 1999, Beyond the desert 1999, pp. 853–867
42. T. Montaruli. Search for WIMPS using upward-going muons in MACRO, Proceedings of the 26th ICRC in Salt Lake City, hep-ex/9905021, pp. 277–280, 17–25 August 1999
43. A. Habig, Discriminating between nu/mu – nu/tau and nu/mu – nu (sterile) in atmospheric nu/mu oscillations with the Super-Kamiokande detector, Proceedings of the 27th ICRC, Hamburg, Germany, hep-ex/0106024, 7–15 August 2001
44. L. Thompson, Dark matter prospects with the antares neutrino telescope, talk given at the Conference Dark 2002, Cape Town, South Africa 4–9 February 2002
45. J. Edsjo, Swedish astroparticle physics, talk given at the Conference Partikeldagarna, Uppsala, Sweden, March 6, 2001
46. J.R. Ellis, T. Falk, K.A. Olive, M. Srednicki, Astropart. Phys. **13**, 181 (2000)
47. V. Bertin, E. Nezri, J. Orloff, in preparation
48. Lars Bergstrom, Joakim Edsjo, Paolo Gondolo, Phys. Rev. D **58**, 103519 (1998)
49. John R. Ellis, Andrew Ferstl, Keith A. Olive, Phys. Lett. B **481**, 304 (2000)
50. John R. Ellis, Andrew Ferstl, Keith A. Olive, Phys. Lett. B **532**, 318 (2002)
51. Vernon D. Barger, Francis Halzen, Dan Hooper, Chung Kao, Phys. Rev. D **65**, 075022 (2002)
52. L. Roszkowski, R. Ruiz de Austri, T. Nihei, JHEP **08**, 024 (2001)
53. Howard Baer, Frank E. Paige, Serban D. Protopopescu, Xerxes Tata, Isajet 7.48: A Monte Carlo event generator for p p, anti-p p, and e+ e- reactions, bnl-het-99-43, fsu-hep-991218, uh-511-952-00, hep-ph/0001086, 1999